NASA Technical Memorandum 83322

Solid Particle Impingement Erosion Characteristics of Cylindrical Surfaces, Pre-Existing Holes and Slits

P. Veerabhadra Rao and Donald H. Buckley
Lewis Research Center
Cleveland, Ohio

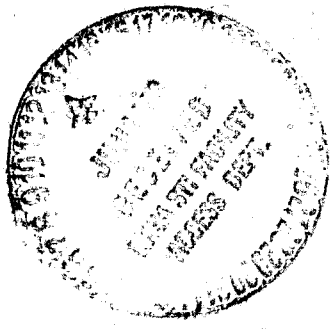

Prepared for the
Cavitation and Multiphase Flow Forum
sponsored by the American Society of Mechanical Engineers
Houston, Texas, June 20–22, 1983

NASA

SOLID PARTICLE IMPINGEMENT EROSION CHARACTERISTICS OF CYLINDRICAL SURFACES, PRE-EXISTING HOLES AND SLITS

P. Veerabhadra Rao* and Donald H. Buckley

National Aeronautics and Space Administration
Lewis Research Center
Cleveland, Ohio 44135

SUMMARY

Solid impingement erosion of ductile materials is detrimental to components of cyclones, gas turbines, rocket tail nozzles, etc. Most experimental studies have been conducted on flat surfaces. The surfaces in real erosion situations, from pneumatic transport to space travel, most frequently involve curvatures - convex and concave. In many devices the progression of erosion in damage prone joints, such as corners and attachments of components, severely limits life. This two part study considered cylindrical surfaces and surfaces with pre-existing holes.

In the first part, the erosion characteristics of aluminum cylinders sandblasted with both spherical and angular erodent particles was studied. The results were compared with those from previously studied flat surfaces. The cylindrical results are discussed herein with respect to impact conditions. The relationship between erosion rate and pit morphology (width, depth, and width to depth ratio) is established. The aspects of (a) erosion rate versus time curves on cylindrical surfaces, (b) long-term exposures, and (c) erosion rate versus time curves with spherical and angular particles are presented.

The second part of the study concerned the erosion morphology and characteristics of aluminum surfaces with pre-existing holes, namely, circular cylindrical and conical holes of different sizes. These studies were conducted with weight loss measurements, scanning electron microscope (SEM), a profilometer, and a depth gage. The morphological features, namely, radial and concentric rings, are discussed with reference to flat surfaces. The similarities and differences of erosion and morphological features are highlighted. The erosion versus time curves of various shapes of holes are discussed and are compared with those of a flat surface. The erosion process at slits is also discussed.

E-1526

INTRODUCTION

Solid impingement erosion of ductile materials is detrimental to equipment such as cyclones, pneumatic pipe lines, boiler units, gas turbines, separators, rocket tail nozzles, valves, bends, etc. Several studies have been conducted using sandblast equipment, wear chambers, wear pumps and nozzles, jet and rotating arm devices to determine the effect of impact velocity, impingement angle, particle size and shape (angularity), abrasive charge, etc. on erosion (refs. 1 and 2).

---

*NRC-NASA Research Associate.

Most of the laboratory studies have considered flat surfaces as test specimens (e.g., refs. 3 and 4). Despite a vast amount of accumulated data on erosion of ductile materials, no universally accepted method of testing or procedure directly available for field application exists.

The surfaces in real erosion situations, from pneumatic transport to space travel, are continuously encountering curvature - convex and concave. The erosion prone joints, corners and attachments of components of the machinery and devices, impart severe life limitations due to the progression of erosion. Some investigators have therefore studied the erosion phenomenon for a specific requirement using particular configurations (refs. 5 and 6). Some researchers have studied cylinders of different materials both along and perpendicular to the axis. For example, Neilson and Gilchrist (ref. 5) tested hard steel, mild steel, brass, and aluminum cylinders using 500-μm iron grit and brass using 250-μm grit. Tilly (ref. 7) tested aluminum cylinders with 60- to 125-μm quartz grit. Also tested were tubes of aluminum oxide using aluminum oxide grit (ref. 5) and tubes of aluminum using 270-μm steel shot (ref. 8). In all these studies the erodent particles have impinged the surface perpendicular to the axis of the cylinder. Carter, et al. (ref. 9), however, tested copper and stainless steel cylinders along their axes using 0.1-mm sand grit.

In sand or air blast tests the jet flow nearing the target deflects from the free-stream trajectory. Small particles, 5 μm or less, are deflected to the greatest degree, and some may miss the surface altogether (refs. 7 and 10). Tilly (ref. 7) has defined the number of particles that strike the target relative to the total initial number as the strike efficiency. He calculated the strike efficiency for various sizes of particles as a function of velocity on cylindrical surfaces and as a function of the angle of approach for flat surfaces in uniform flows.

The aerodynamic effects involved during normal incidence in a uniform flow have been recently discussed by Laitone (refs. 11 and 12) and Murthy and Crowe (ref. 13). Laitone (ref. 14), however, also considered the particle rebound phenomenon around a cylinder. Most of these studies have not, however, considered those aspects needed to bring forward detailed information on erosion behavior for general applications. The time effects and the morphological features of the erosion process on cylindrical surfaces and holes which affect friction and drag characteristics have not been reported.

The objective of this paper is to present erosion data for aluminum alloy cylinders exposed to a jet of microglass beads and angular crushed glass particles. The study reports erosion and erosion rate with respect to morphological features. The erosion characteristics of conical and circular cylindrical holes of different size as well as slits are also presented.

NOMENCLATURE

A,A'	coefficients
a	constant (intercept)
b	base diameter of cylindrical hole
C	coefficient (Eqs. (6) and (7))
c	coefficient (Figs. 10 and 14)
D	diameter of circular cylindrical hole
d	depth of pre-existing hole
m	exponent
n	exponent

t exposure time
V cumulative volume loss
w abrasive charge

Subscript:

max maximum

APPARATUS AND EXPERIMENTAL PROCEDURE

Specimens

Specimens of the aluminum alloy, 6061-T6511 were used in this investigation. The aluminum cylinders of 12.7- and 25.4-mm diam and 37.5-mm long were used. Both circular cylindrical and geometrically similar conical holes were drilled on the 6- by 25- by 37.5-mm aluminum alloy specimens. The nominal composition and mechanical properties of the aluminum alloy are available in (ref. 15). Before erosion exposure, all specimens were polished with 600-grit emery paper, then with 3 μm diamond paste, cleaned with distilled water, and air dried.

Apparatus and Procedure

A sand-blasting facility was used to continuously impact test specimens at normal incidence. Commercial grade no. 9 (20 μm diam) spherical microglass beads and commercial grade no. 10 (30 μm) angular crushed glass were used. The particle size distribution of glass beads has been presented in (ref. 16). The SEM micrographic details of the sizes and shapes of both forms of glass are available in literature (refs. 17 and 18). In the sand-blasting facility the distance between the specimen and the nozzle (1.18 mm diam) was 13 mm. Argon was used as the driving-gas at gage pressures of 0.27 and 0.82 MPa. The average particle velocities and erodent flow rates are presented in table I. The velocities are obtained by using a double disk arrangement similar to one discussed earlier (ref. 19). The jet divergence was about ±2° relative to the center line. The nozzle is replaced frequently during the experiments to limit the effect of nozzle wear on jet divergence, particle velocity, erodent flow rate, etc. The nonsymmetric erosion pit is an indirect and approximate indication of the nozzle wear in this type of study.

Volume loss was obtained by weighing specimens before and after exposure to the erodents and dividing by density. The sensitivity of the balance was ±0.1 mg. Surface profiles of the eroded surfaces were recorded with a profilometer. The depth of the shallow pits were measured from surface traces and checked with a depth gage. The deep pits were always measured with a depth gage. The sensitivity of the gage is ±2.5 μm (0.0001 in.). The eroded surfaces were observed with an SEM.

EXPERIMENTAL RESULTS AND DISCUSSION

The experimental results are presented in two parts. First, the erosion of circular cylinders which represent features of blunt leading edges as in gas turbine blades. Second, the erosion characteristics of circular cylindrical and conical holes, as well as slits which represent asperities, joints, corners and attachments on erosion prone surfaces.

Erosion of Circular Cylinders

Erosion characteristics. - Figure 1 presents cumulative erosion of 25.4- and 12.7-mm-diameter aluminum alloy circular cylinders as a function of the flow of the spherical glass bead and angular crushed glass. The driving gas pressure was 0.82 MPa. Results obtained on flat surfaces (refs. 17 and 20) were included for comparison. Figure 1 shows that the erosion of cylinders exposed perpendicular to their axis is less than the erosion of flat surfaces. This is true for both forms of glass. This is also in agreement with earlier investigations (refs. 7 and 10) which attributed this effect to the reduction of strike efficiency in a uniform flow of erodent particles.

As the diameter of the cylinder decreased, the cumulative erosion also decreased (see fig. 1). Most impinging jets induce damage by direct impact and radial outflow of the particles. On slightly convex surfaces, as cylinders, the radial outflow component of erosion is believed to be reduced. Also, the particles deflected at a stagnation point, as discussed by earlier investigators (refs. 7, 11, and 12), may possibly miss the surface altogether. Hence, on cylinders, the angle of impingement changes from normal (90°), to glancing (0°), or to complete missing. This probably causes the reduction in erosion. Although other researchers (refs. 5 and 7) have studied the erosion characteristics of circular cylinders, the effect of time and jet have not been reported.

Strike efficiency. - The reduction of erosion and strike efficiency of particles from a jet impinging a cylindrical surface may be attributed to the change of angle of incidence when compared with flat surfaces (see schematic in fig. 1). Thus, both the radial out-flow pattern and the course of some particles are changed, and some particles escape hitting the surface (refs. 7 and 10). The ratios of strike efficiency on a flat surface to that on a cylindrical surface for uniform flows of 20- and 30-μm size particles, without considering shape, were calculated to be 1.103 and 1.05, respectively (ref. 7). The flat surface to cylindrical surface erosion rate ratios from steady-state regions for jet flow glass beads (20 μm) and crushed glass (30 μm) were 1.105 and 1.002 (fig. 1). This agreement with glass beads shows that surface configuration seems to be of considerable influence during the erosion process. During the glass bead impingement, material appears to have been removed in the form of flakes as shown in figure 2. Individual dents are also seen clearly in figures 2(c) and (d). These flakes are believed to be formed by cyclic stress, deformation, extrusion, and fatigue failure. This mechanism is generally referred to as deformation wear phenomenon (ref. 15). The disagreement for crushed glass particles, however, indicates that the surface configuration, at least in the present study, does not seem to be of much influence during erosion, most probably because of the cutting wear phenomenon with angular particles. During cutting wear (ref. 15), all surfaces of the test specimens exhibit jagged, angular faceted patterns as shown in figure 3. In this case, surface appears to be cut by impact and subsequent outflow.

Erosion rate versus time curves. - Figure 4 presents volume loss rate versus abrasive charge curves. The different periods of erosion observed in general may be defined as follows (ref. 21):

(a) Incubation period - the time span or dosage of erodent particle mass during which there is little or no weight loss, in fact, in a few cases there can be a slight weight gain due to the embedment or deposition of particles. This period is sometimes referred to as the induction period.

(b) Acceleration period - the time span or erodent particle dosage during

which the weight loss rate increases gradually or rapidly.

(c) Deceleration period - the time span or erodent particle dosage during which weight loss rate decreases rapidly.

(d) Steady-state period - the time span or erodent particle dasage during which weight loss rate becomes constant and continues constant for a long time (fig. 4(a)). This period is also commonly referred to as the maximum rate.

(e) Peak erosion rate - the erosion rate observed between acceleration and deceleration periods (fig. 4(b)). This is the maximum rate.

The surface configuration does not seem to influence the individual shape of the erosion rate versus abrasive charge curve for individual forms of glass particles. Curves similar to those in figure 4(a) have been discussed by several investigators, e.g., (refs. 3, 7, and 9). The shape of the curve in figure 4(b) is a less frequent type and has not been reported earlier except by the present investigators (ref. 21).

To explore the behavior of flat and cylindrical surfaces with respect to cumulative erosion, instantaneous and cumulative average erosion rates were plotted as functions of erosion volume loss (fig. 5). These plots indicate that at a particular volume loss the flat surfaces still have higher erosion rates than the circular cylinders. It seems that erosion peaks occur earlier on flat surfaces than on the cylinders with both forms of glass.

Morphological features on cylinder. - Five and four different regions have been observed on flat surfaces during spherical glass bead[1] and crushed glass[2] impingement, as shown in figures 6 and 7, respectively. These patterns are also observed on cylindrical surfaces. The radial tracks on sloping cylindrical surfaces are, however, less severe.

Analysis of depth, width and width to depth ratio of pits indicates that the pit width versus time or pit depth versus time curves seem to be similar to erosion versus time curves for glass bead impingement. The pit depth rate versus time curves are similar to erosion rate versus time curves for crushed glass impingement. Pit depth rate apparently controls erosion rate to a larger extent than do the width rate and width to depth ratio of the pit for crushed glass impingement as recently observed by the authors (ref. 21).

Long-term exposures. - In energy conversion systems erosion prone components are exposed to long term (around 20 000 hr) erosive environments. Figure 4 shows that the erosion rate does not change for spherical erodent

---

[1]Flat specimens exposed to glass bead impingement, at an advanced stage, (fig. 6), exhibit five regions (ref. 17): Region 1 consists mainly of radial deformation tracks, emanating from the center of the impact. The depth and width of the tracks increase with radial distance from the center of the pit. Region 2 consists of both radial tracks and concentric rings. For convenience, these have been called "radial-concentric" rings. It was believed to be the first observation of such patterns. Region 3 is a steep-slope region composed mainly of radial tracks. Region 4 is a rougher, with irregular concentric, ripple, and crest patterns. Region 5 is a transition from the undamaged zone to the incipient erosion zone.

[2]Flat surfaces exposed to crushed glass particle impingement, at an advanced stage (fig. 7), exhibit four regions (ref. 20): Region 1, pit bottom with no clear pattern; region 2, concentric ripple patterns on the sides of the pit; region 3, a rough undulating region with a changing slope from almost vertical to horizontal; and region 4, the transition from incipient erosion zone to the undamaged area of the specimen.

particles and continuously decreases for angular erodent particles. Figure 4(b) may be more realistic as most of the particles encountered in real situations are angular. Also, for components where erosion is prevalent, this may give the design engineers an estimate not only of how to predict erosion but also to use highly resistant material to reduce breakdown or component change time. It is evident with angular particles that for long exposures the pit becomes sufficiently deep to affect the erosion rate.

Unification of curves. - Curves in figure 4 represent two different characteristics: One with incubation, acceleration, and steady-state periods (fig. 4(a)), and a second with incubation, acceleration, peak erosion, and deceleration periods (fig. 4(b)). In this section a method is suggested to bring the results of individual types to a unified form. The analysis method is shown schematically in figures 8 and 9. Curves A to D in figure 8(a) represent one type of erosion rate versus time curve (as in fig. 4(a)) and curves E to H in fig. 8(b) represent the other type (as in fig. 4(b)).

The instantaneous or cumulative average erosion rate of each curve is normalized by first setting both the maximum erosion rate (steady-state or peak erosion rate) and the time of abrasive charge to reach this peak to 1, and then determining the ratios of all other erosion rates and times or abrasive charges to the peaks (fig. 9). Statistically constructed or experimentally obtained scatter bands can therefore be drawn to include the percentage deviation in experimental data.

These unified curves may be used for correlating different types of materials and laboratory tests with each other and with field data. With a knowledge of only two parameters (a) peak or steady-state erosion rate, and (b) time of abrasive charge to attain this peak, the erosion rates can be calculated or predicted. Long-term erosion predictions, which are necessary in energy conversion system components, can therefore be made more accurately from only a few data points.

Characteristic of erosion rate versus cumulative erosion curve. - Figure 10 presents typical log-log plots of cumulative average erosion rate versus erosion of an aluminum alloy cylinder and an aluminum alloy flat impacted with glass beads. The acceleration stage of erosion may be represented by a power law

$$\frac{V}{t} = A' V^n \tag{1}$$

or

$$\frac{V}{w} = A\, V^n \tag{2}$$

or

$$V = (Aw)^{\frac{1}{(1-n)}} \tag{3}$$

where V is the cumulative volume loss (in mm^3), t is the exposure time (in min) corresponding to V, w is the abrasive charge (in g) corresponding to V, A' and A are coefficients, and n is an exponent. The coefficients, exponents (slopes), and correlation coefficients are marked in figure 10. Differentiation of equation (3) with respect to w provides

$$\frac{dV}{dw} = \frac{A\, V^n}{(1 - n)} = \frac{V}{[(1 - n)w]} \tag{4}$$

$$\frac{dV}{dt} = \frac{V}{[(1 - n)\ t]} \tag{5}$$

Equation (5) indicates that instantaneous erosion rate, dV/dw or dV/dt, during the acceleration stage may always appear to be a function of cumulative average erosion rate, V/w or V/t. The ratio of these two rates are therefore constant. Substitution of equation (3) into equation (4) results in

$$\frac{dV}{dw} = Cw^m \tag{6}$$

$$C = \frac{A^{\frac{1}{(1-n)}}}{(1 - n)} \tag{7}$$

where

$$m = \frac{n}{(1 - n)} \tag{8}$$

The advantage of this relation is that values of $(dV/dt)_{max}$ and time or abrasive dosage corresponding to this peak may be calculated with just a few experimental points and with a knowledge of A, n, and V/t. The experimental points of power law relation deviate exactly at $(V/t)_{max}$. Hence, the value of time corresponding to the peak may therefore be calculated. This type of power law relation, and the characteristics of erosion versus time and erosion rate versus time curves require further investigation.

Erosion of Pre-Existing Holes and Slits

Morphological features of holes. - Figures 11 to 13 present a series of SEM micrographs of aluminum alloy specimens with pre-existing conical holes as a function of exposure to glass bead impingement time. The driving gas pressure of 0.27 MPa is considered to systematically reveal morphological features. These holes are geometrically similar with a constant aspect ratio (base diameter b to depth d) of 2. The existence of five regions as discussed by the authors (ref. 17) and as observed in figure 6 for a flat surface is also seen in the present study. An SEM micrograph shown in figure 14 at 0.27 MPa gas pressure condition do not however show complete development of radial concentric rings in region 2.

The main features observed with conical holes are that radial tracks form almost immediately and concentric ripples (in region 4) are very faint. The inception of radial-concentric rings are seen in figures 12 and 13. From the micrographs it appears that damage on small pits is more than on deep pits. However, this seems to be true only during the initial phases of erosion, as shown in figure 15, which presents cumulative erosion versus time curves.

Figures 16 to 18 present a series of SEM micrographs of aluminum alloy specimens with circular cylindrical holes as a function of exposure to glass bead impingement time. The driving gas pressure is 0.27 MPa. For small holes, radial tracks are observed around the top of the hole (fig. 16). Radial, concentric rings always appear to develop on the side of the hole, and the central portion of hole contains only irregular patterns. For larger

diameter holes, the radial tracks form at the bottom of the pit (figs. 17 and 18). Irregular circumferential ripple patterns are also seen at the pit bottom for wide pits (fig. 18). The radial tracks and radial, concentric rings appear to form earlier at 3.18 and 6.35 mm diameters than on a flat surface. Hence, more erosion is expected on these types of surfaces.

Figure 19 presents erosion versus time curves for circular cylindrical holes of constant depth, d (1.35 mm) and diameters D of 3.18, 6.35, and 11.12 mm. It is evident that erosion is large on the two small diameters.

Erosion characteristics. - It is evident from figures 15 and 19 that the erosion of aluminum alloy surfaces with holes -- conical and circular cylindrical -- appears to be always more than the erosion on the flat surface except when the hole is very wide. However, there seems to be a different trend for these two forms of holes. The steady-state erosion rate increases with increases in the size of the conical holes (keeping the same aspect ratio, b/d) and with decreases in the diameter of cylindrical holes (keeping approximately constant depth) (fig. 1). The radial outflow pattern seems to be the main reason for the differences in erosion resistance. Additional studies on scale effects is in progress.

Erosion at holes, edges, and narrow slits. - The erosion rate at holes and edges of the test specimens was considerably higher than that for a flat surface in the present study (figs. 15 and 19). Figure 20 presents a typical plot of erosion at a narrow slit (0.1 mm) with respect to exposure time of crushed glass flow. This figure indicates that cumulative volume loss at a narrow slit is less than that on flat surfaces, although erosion progressed fast through the slit. This result, which contradicts that from shallow holes, is due mainly to the observed erosion below the slit on the neighboring component. Hence, slits reduce erosion but extend or transfer the process to the adjoining or underlying components and base materials.

Figure 20 shows that slopes of the curves for both flat surfaces - with and without slits - are the same. It is generally observed that with slits the depth of the pit increases faster than the width of the pit. Hence, one may assume that most impinging particles do not outflow from the pit surface, but escape through the slit to adjoining components, possibly causing erosion inside.

CONCLUSIONS

The main observations of these studies are as follows:

1. Circular cylindrical surfaces experienced less erosion than flat surfaces with both glass bead and crushed glass impingement particles. The uniform-flow strike efficiency proposed also agrees with glass bead jets, providing almost the same ratio of erosion rate between flat and cylindrical surfaces.

2. Curves of erosion rate versus time or glass bead dosage for circular cylinders exhibited incubation, acceleration, and steady-state periods. With crushed glass impingement, they exhibited incubation, acceleration, peak erosion, and deceleration periods.

3. A normalization method was suggested for the individual type of curves with respect to peak erosion rate and time or abrasive dosage corresponding to the peak. This technique is believed to unify the curves and facilitate prediction.

4. A power law relation was observed between cumulative average erosion rate and volume loss during the acceleration stage of erosion. This is believed to be advantageous for characterizing erosion using fewer experimental points.

5. Most of the pre-existing holes - circular cylindrical and conical - exhibited more erosion than flat surfaces.

6. The morphological features on an aluminum surface with holes were similar to the ones on flat surfaces. The radial tracks were, however, observed on conical surfaces immediately after exposure to glass bead impingement.

7. The erosion at a narrow slit was less than that on a flat surface. A slit generally extends the erosion to the adjoining and underlying components and base materials.

REFERENCES

1. National Materials Advisory Board, "Erosion Control in Energy Systems," NMAB-334, Washington, D.C., 1977.

2. Adler, W. F., "Assessment of the State of Knowledge Pertaining to Solid Particle Erosion," Rept. ETI CR 79-680, Contract DAAG 29-77-C-0039, U.S. Army Research Office, 1979.

3. Finnie, I., Wolak, J., and Kabil, Y., "Erosion of Metals by Solid Particles," Journal of Materials, Vol. 2, Sept. 1967, pp. 682-700.

4. Soderberg, S., et al., "Erosion Classification of Materials using a Centrifugal Erosion Tester," Tribology International, Vol. 14, No. 6, Dec. 1981, pp. 333-343.

5. Neilson, J. H., and Gilchrist, A., "An Experimental Investigation into Aspects of Erosion in Rocket Motor Tail Nozzles," Wear, Vol. 11, 1968, pp. 123-143.

6. Grant, G., and Tabakoff, W., "Erosion Prediction in Turbomachinery Resulting from Environmental Solid Particles," Journal of Aircraft, Vol. 12, No. 5, May 1975, pp. 471-478.

7. Tilly, G. P., "Erosion Caused by Airborne Particles," Wear, Vol. 14, 1969, pp. 63-79.

8. Maji, J, and Sheldon, G. L., "Mechanisms of Erosion of a Ductile Material by Solid Particles," Erosion: Prevention and Useful Applications, ASTM STP 664, W. F. Adler, Ed., American Society for Testing and Materials, Philadelphia, 1979, pp. 136-147.

9. Carter, G., Nobes, M. J., and Arshak, K. I., "The Mechanism of Ripple Generation on Sandblasted Ductile Solids," Wear, Vol. 65, 1980, pp. 151-174.

10. Tilly, G. P., "Erosion by Impact of Solid Particles," Treatise on Materials Science and Technology, Vol. 13, D. Scott, Ed., Academic Press, New York, 1979, pp. 287-319.

11. Laitone, J. A., "Aerodynamic Effects in the Erosion Process," Wear, Vol. 56, No. 1, Sept. 1979, pp. 239-246.

12. Laitone, J. A., "Erosion Prediction near a Stagnation Point Resulting from Aerodynamically Entrained Solid Particles," Journal of Aircraft, Vol. 16, No. 12, Dec. 1979, pp. 809-814.

13. Murthy, J., and Crowe, C. T., "Aerodynamic Effects on the Erosion of Finite Size Targets," Particulate Laden Flows in Turbomachinery, W. Tabakoff, C. T. Crowe and D. R. Cale, eds., American Society of Mechanical Engineers, New York, 1982, pp. 43-48.

14. Laitone, J. A., "Characterization of Particle Rebound Phenomena in the Erosion Turbomachinery," LBL-12017, Lawrence Berkley Laboratory, 1979.

15. Veerabhadra Rao, P., Young, S. G., and Buckley, D. H., "A Study of the Nature of Solid Particle Impact and Shape on the Erosion Morphology of Ductile Metals," NASA TM 82933, July 1982.

16. Veerabhadra Rao, P., Young, S. G., and Buckley, D. H., "Solid Spherical Glass Particle Impingement Studies of Plastic Materials," NASA TP 2161, 1983.

17. Veerabhadra Rao, P., Young, S. G., and Buckley, D. H., "Morphology of Ductile Metals Eroded by Spherical Particle Impingement at Normal Incidence," Wear, Vol. 85, 1983, pp. 223-237.

18. Salik, J., and Buckley, D. H., "Effect of Erodent Particle Shape and Various Heat Treatments on Erosion Resistance of Plain Carbon Steel," NASA TP-1755, 1981.

19. Ruff, A. W., and Ives, L. K., "Measurement of Solid Particle Velocity in Erosive Wear," Wear, Vol. 35, 1975, pp. 195-199.

20. Veerabhadra Rao, P., Young, S. G., and Buckley, D. H., "Morphology of an Aluminum Alloy Eroded by Angular Particle Impingement at Normal Incidence," NASA TP 2139, 1983.

21. Veerabhadra Rao, P., and Buckley, D. H., "Time Dependence of Solid Jet Impingement Erosion of an Aluminum Alloy," NASA TP 2169, 1983.

TABLE 1. - PARTICLE VELOCITY AND FLOW RATE OF GLASS BEADS AND CRUSHED GLASS PARTICLES

Parameter	Parameter corresponding to erodent particles flowing at gas pressure			
	Glass beads		Crushed glass	
	0.27 MPa	0.82 MPa	0.27 MPa	0.82 MPa
Particle velocity, m/sec	72	130	48	87
Particle flow rate, g/sec	0.98	0.48	0.34	0.22

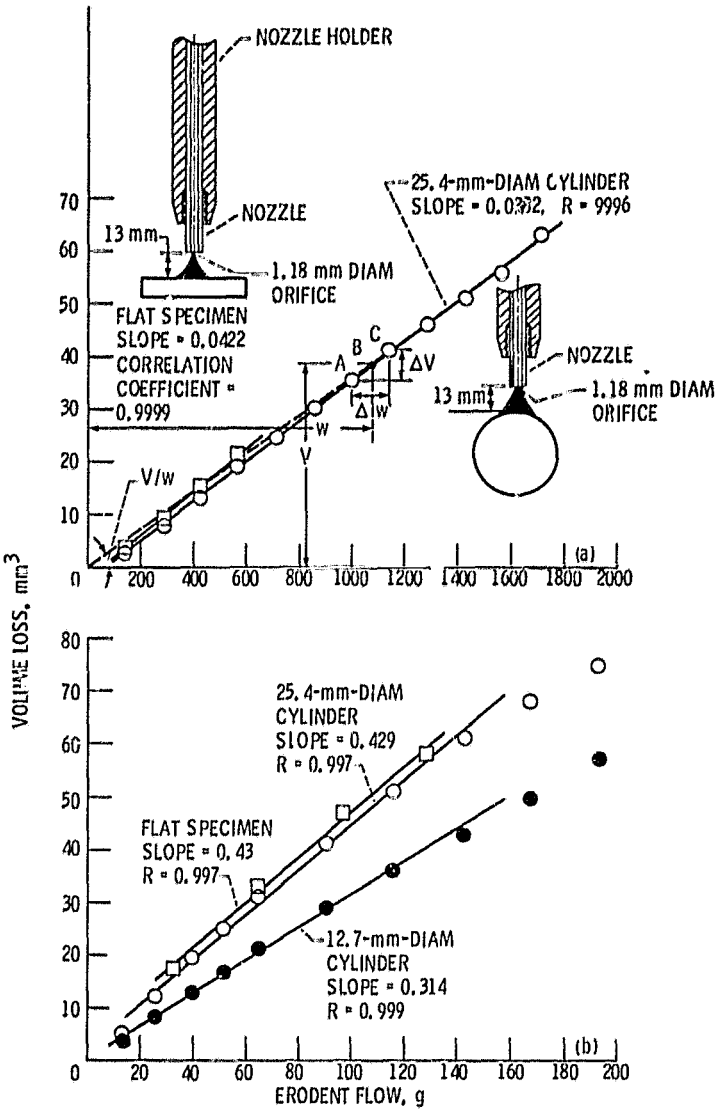

(a) Glass beads.

(b) Crushed glass.

Figure 1. - Cumulative volume loss as a function of erodent impingement on circular cylinders and flat surface at normal incidence. Driving gas pressure, 0.82 MPa (gage). Instantaneous erosion rate at B equals slope of local tangent at B = $\Delta V / \Delta w$; cumulative average erosion rate at B equals slope of line joining origin and point B = V / w. Experimental data variation is $\pm$ 7.76 percent.

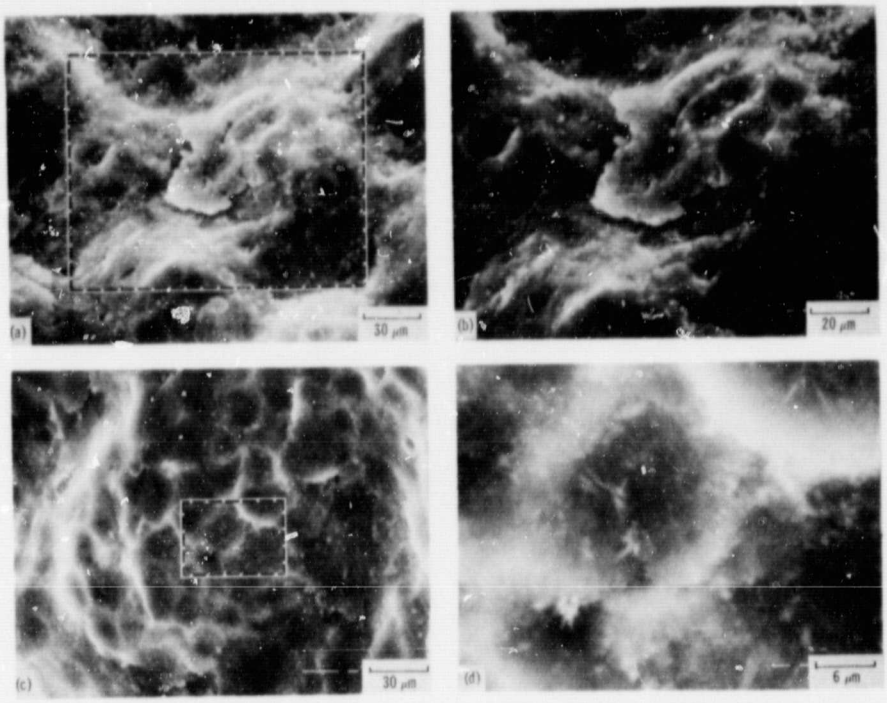

(a) Disloding flakes.

(b) Detailed view of flake in (a).

(c) Individual flakes and dents.

(d) Detailed individual dents in (c).

Figure 2. - SEM micrographs of eroded aluminum alloy surfaces exposed to glass bead impingement depicting flakes and dents.

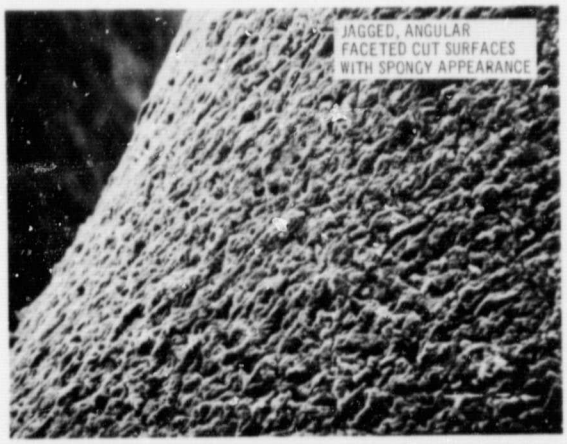

Figure 3. - SEM micrograph of eroded aluminum alloy surface exposed to crushed glass impingement depicting jagged and cut surfaces.

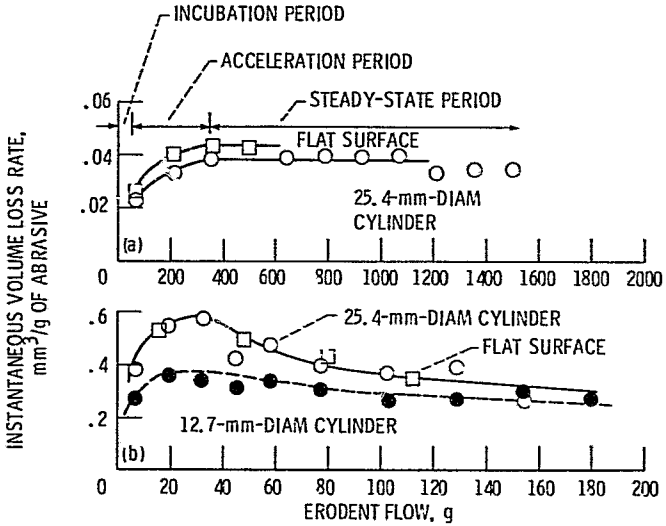

(a) Glass bead impingement.

(b) Crushed glass impingement.

Figure 4. - Instantaneous volume loss rate as function of erodent impingement on circular cylinders and flat surfaces at normal incidence. Driving gas pressure, 0.82 MPa.

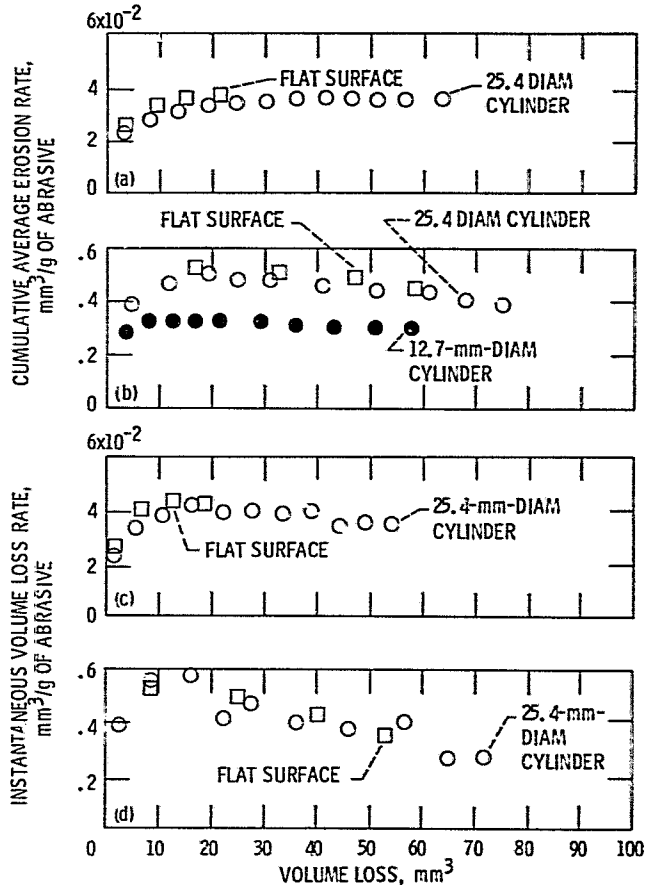

(a) Glass beads.

(b) Crushed glass.

(c) Glass beads.

(d) Crushed glass.

Figure 5. - Erosion rate as function of cumulative erosion during impingement of erodents on circular cylinders and flat surfaces at normal incidence. Driving gas pressure, 0.82 MPa.

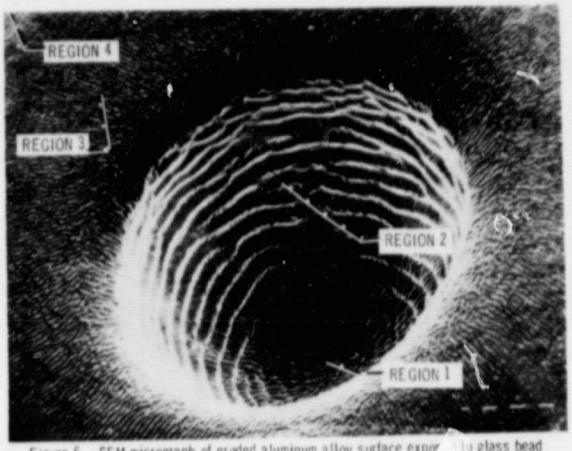

Figure 6. - SEM micrograph of eroded aluminum alloy surface exposed to glass bead impingement. Gas pressure, 0.82 MPa; exposure time, 20 min.

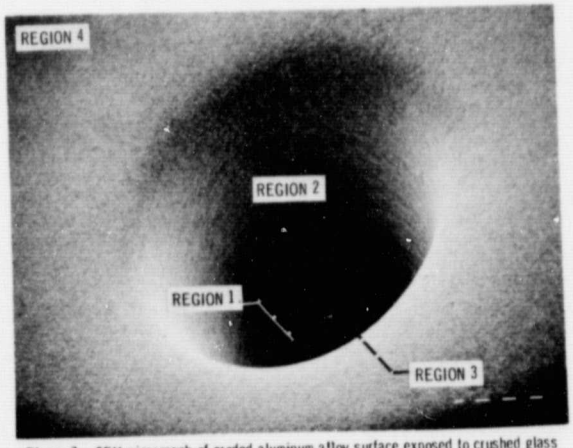

Figure 7. - SEM micrograph of eroded aluminum alloy surface exposed to crushed glass impingement. Gas pressure, 0.82 MPa; exposure time, 20 min.

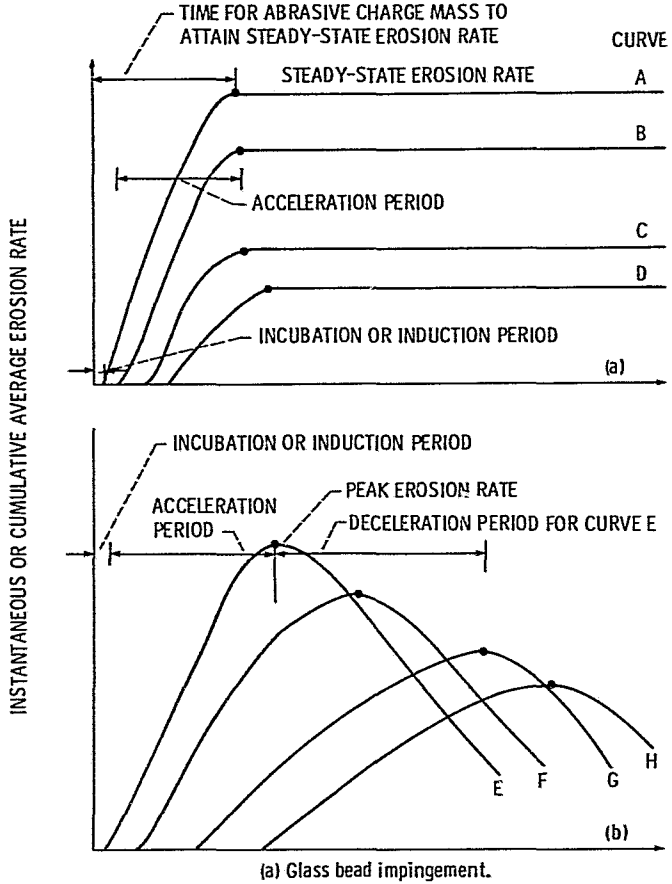

(a) Glass bead impingement.

(b) Crushed glass impingement.

Figure 8. - Typical instantaneous or cumulative average erosion rate versus time or abrasive mass curves.

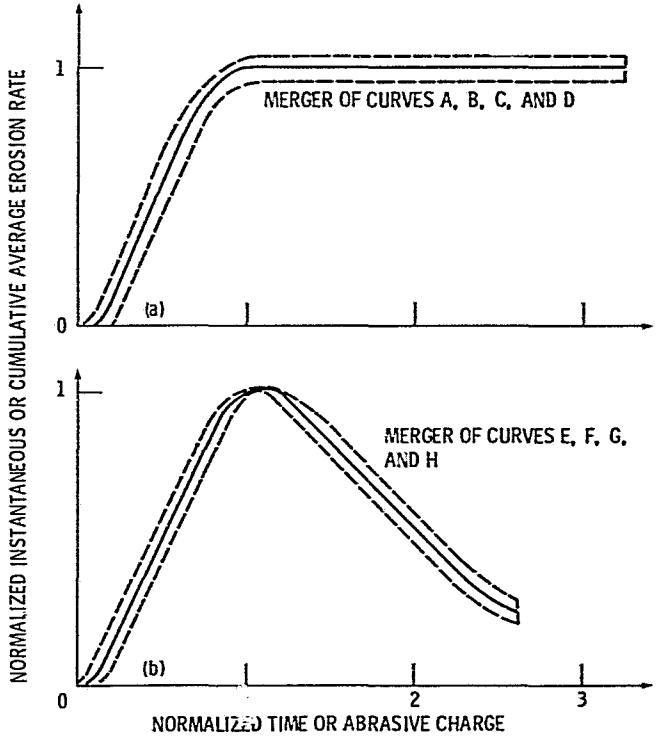

(a) Glass bead impingement.

(b) Crushed glass impingement.

Figure 9. - Unified normalized erosion rate versus normalized time or abrasive charge curves.

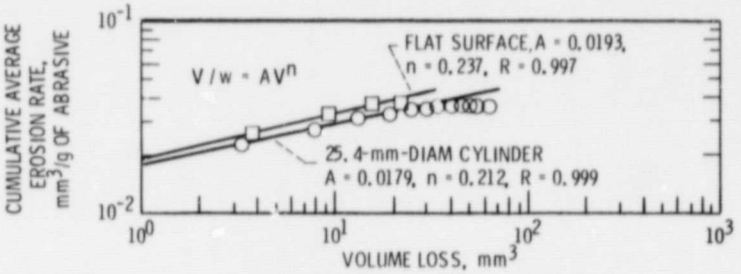

Figure 10. - Cumulative average erosion rate versus volume loss curves of aluminum cylinder and flat surface during glass bead impingement. Driving-gas pressure, 0.82 MPa.

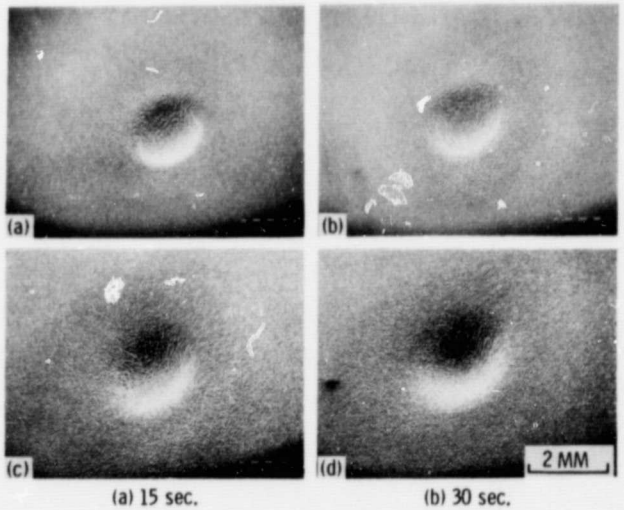

(a) 15 sec. (b) 30 sec.
(c) 120 sec. (d) 180 sec.

Figure 11.- SEM micrographs of eroded aluminum surfaces with conical hole (b = 0.76 mm and d = 0.38 mm) exposed to glass bead impingement. Driving-gas pressure, 0.27 MPa.

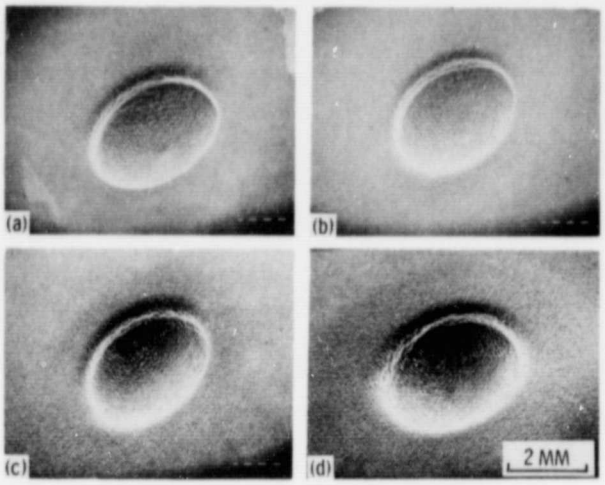

(a) 15 sec. (b) 30 sec.
(c) 120 sec. (d) 180 sec.

Figure 12.- SEM micrographs of eroded aluminum surfaces with conical hole (b = 1.97 mm and d = 0.98 mm) exposed to glass bead impingement. Driving-gas pressure, 0.27 MPa.

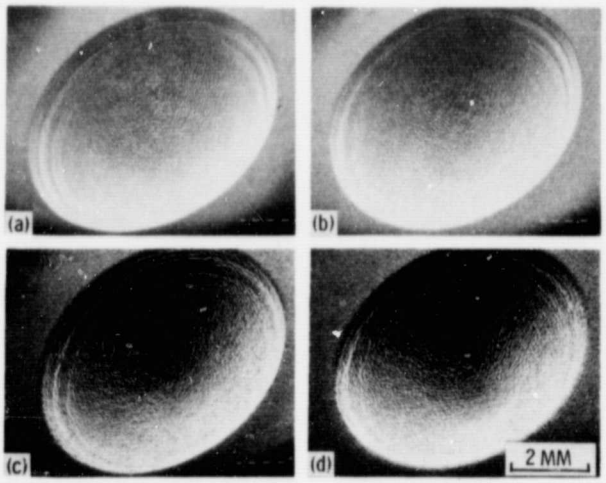

(a) 15 sec. (b) 30 sec.
(c) 120 sec. (d) 180 sec.

Figure 13.- SEM micrographs of eroded aluminum surfaces with conical hole (b = 3.07 mm and 1.53 mm) exposed to glass bead impingement. Driving-gas pressure, 0.27 MPa.

Figure 14. - SEM micrograph of eroded aluminum alloy surface exposed to glass bead impingement. Gas pressure, 0.27 MPa; exposure time, 20 min.

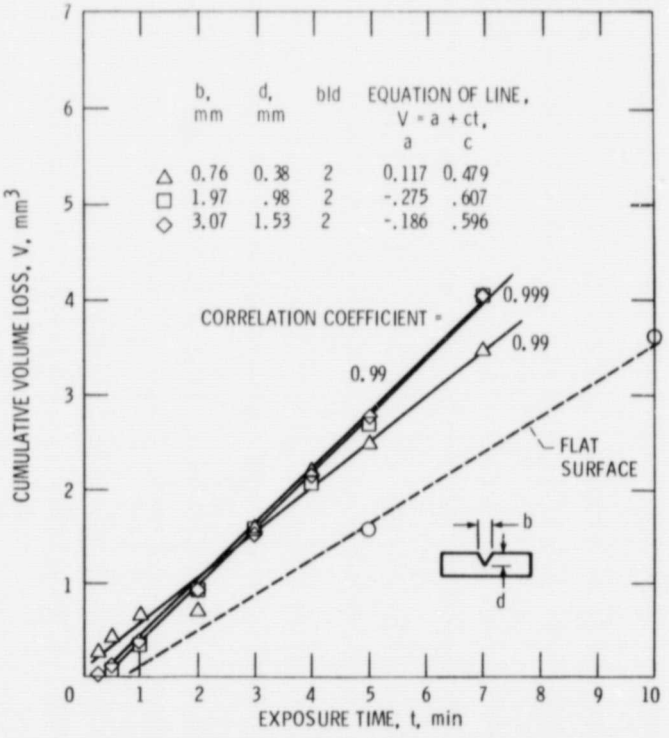

Figure 15. - Erosion of aluminum surfaces with pre-existing conical holes as a function of time. Driving-gas pressure, 0.27 MPa. Experimental deviation, ±6.6 percent.

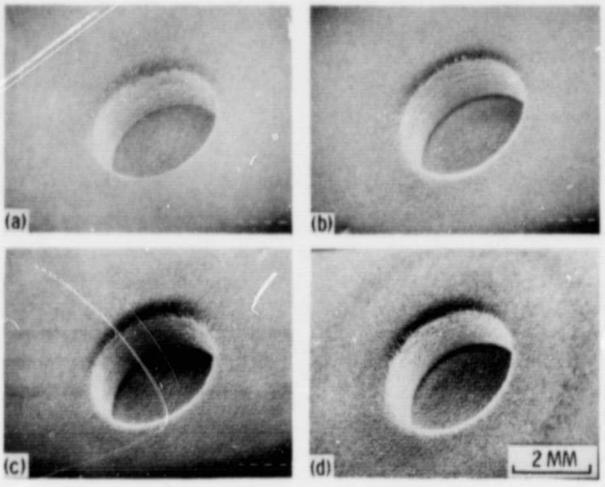

(a) 15 sec. (b) 30 sec.
(c) 60 sec. (d) 120 sec.

Figure 16. - SEM micrographs of eroded aluminum surfaces with circular cylindrical hole (D = 3.18 mm and d = 1.35 mm) exposed to glass bead impingement. Driving-gas pressure, 0.27 MPa.

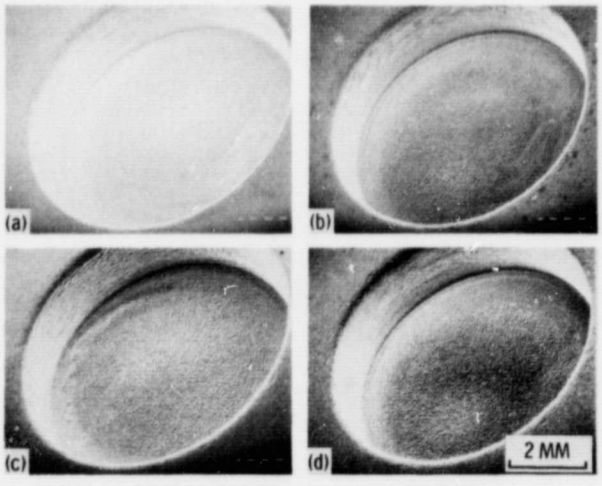

(a) 15 sec. (b) 30 sec.
(c) 60 sec. (d) 120 sec.

Figure 17. - SEM micrographs of eroded aluminum surfaces with circular cylindrical hole (D = 6.35 mm and d = 1.37 mm) exposed to glass bead impingement. Driving-gas pressure, 0.27 MPa.

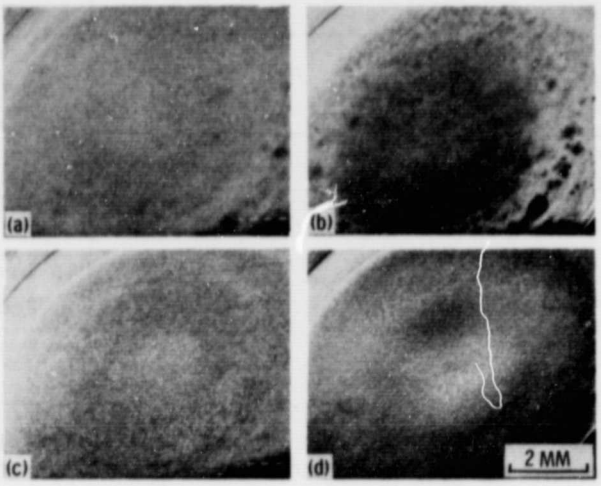

(a) 30 sec. (b) 60 sec.
(c) 120 sec. (d) 360 sec.

Figure 18. - SEM micrographs of eroded aluminum surfaces with circular cylindrical holes (D = 11.12 mm and d = 1.33 mm) exposed to glass bead impingement. Driving-gas pressure, 0.27 MPa.

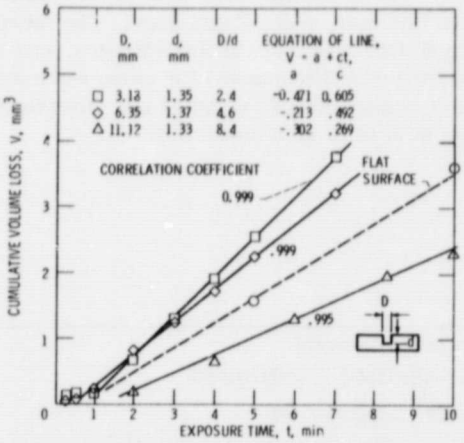

Figure 19. - Erosion of aluminum surfaces with pre-existing circular cylindrical holes as a function of time. Driving-gas pressure, 0.27 MPa. Experimental deviation, ±5.9 percent.

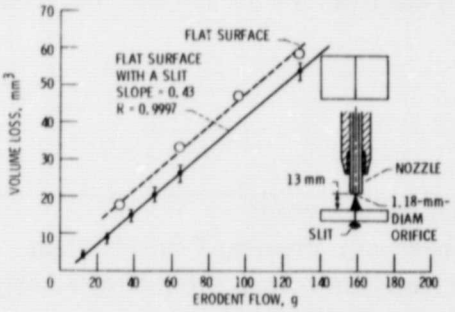

Figure 20. - Cumulative volume loss of aluminum alloy as function of crushed glass impingement on a slit at normal incidence. Driving-gas pressure, 0.82 MPa.